High-resolution ion mobility measurements

Ph. Dugourd,[a] R. R. Hudgins, D. E. Clemmer,[b] and M. F. Jarrold
Department of Chemistry, Northwestern University, Evanston, Illinois 60208

(Received 22 July 1996; accepted for publication 28 October 1996)

Gas phase ion mobility measurements can resolve structural isomers for polyatomic ions and provide information about their geometries. A new experimental apparatus for performing high-resolution ion mobility measurements is described. The apparatus consists of a pulsed laser vaporization/desorption source coupled through an ion gate to a 63-cm-long drift tube. The ion gate is a critical component that prevents the diffusion of neutral species from the source into the drift tube. Ions travel along the drift tube under the influence of a uniform electric field. At the end of the drift tube some of the ions exit through a small aperture. They are focused into a quadrupole mass spectrometer, where they are mass analyzed, and then detected by an off-axis collision dynode and by dual microchannel plates. The apparatus is operated with a drift voltage of up to 14 000 V and a helium buffer gas pressure of around 500 Torr. The resolving power for ion mobility measurements is over an order of magnitude higher than has been achieved using conventional injected-ion drift tube techniques. Examples of the application of the new apparatus in resolving isomers of laser desorbed metallofullerenes, in studying silicon clusters generated by laser vaporization, and in following the isomerization of small nanocrystalline $(NaCl)_nCl^-$ clusters as a function of temperature, are presented.
[S0034-6748(97)01202-1]

I. INTRODUCTION

The mobility of a gas phase ion is a measure of how rapidly it moves through a buffer gas under the influence of an electric field. The mobility of a polyatomic ion depends on its average collision cross section, which in turn depends on its geometry. Thus mobility measurements can be used to separate ions with different geometries. For example, Hagen[1] showed in 1979 that structural isomers of polycyclic aromatic hydrocarbons could be separated on the basis of their different mobilities. For atomic ions the mobility depends on the electronic state, as was shown by Rowe *et al.* in 1980.[2] Ion mobility measurements form the basis of a sensitive and selective analytical technique, ion mobility spectrometry,[3,4] developed by Cohen and Karasek in 1970. Ion mobility spectrometry has been used to detect drugs, chemical warfare agents, explosives, and environmental pollutants.[5] Neural network computer models have been developed to predict mobilities from structural information.[6] Several groups have used mobility measurements to characterize the size distribution of aerosol particles and small metal particles.[7] Ion mobilities also provide important fundamental information about the interaction between ions and molecules.[8] This provided the motivation for early studies of ion mobilities using drift tube techniques. In addition to information about ion mobilities, drift tube studies can provide information about ion–molecule reaction kinetics and equilibria.[9] The injected-ion drift tube, developed by Kaneto, Megill, and Hasted in 1966,[10] has been widely used in these studies. In this technique, mass-selected ions are injected into a drift tube containing a buffer gas, the ions travel across the drift tube under the influence of an electric field, and some exit through a small aperture. The exiting ions are then mass analyzed and detected. This technique has recently been used to study the chemistry of atomic clusters; for example, silicon clusters have been extensively studied using this approach.[11]

In the last few years there has been renewed interest in using ion mobility measurements to deduce structural information about polyatomic ions. Ion mobility measurements can resolve structural isomers and provide an accurate measure of their average collision cross sections. Information about the geometries can then be deduced from the cross sections by calculating orientationally averaged cross sections for assumed geometries for comparison with the measured cross sections. Ion mobility measurements have been used to examine carbon,[12,13] silicon,[14] germanium,[15] and metal-containing carbon clusters.[16] The results for carbon clusters, first studied by Bowers and collaborators, are particularly noteworthy because so many different structural isomers have been resolved. Ion mobility measurements together with a collisional annealing technique[17] have provided insight into the mechanism of fullerene formation.[18]

While covalent clusters have isomers with very different shapes, and hence very different mobilities, for metal clusters and ionic clusters only compact structures with similar collision cross sections are expected. The application of ion mobility measurements to noncovalent clusters has thus been hindered by the low resolution available in injected-ion drift tube experiments. Furthermore, ion mobility measurements have recently been used to examine the conformations of peptides[19] and proteins[20] in the gas phase, and these studies have also been hindered by the low resolution. To overcome this problem we have constructed a new high-resolution ion mobility apparatus. The resolving power achieved with the new apparatus described here is over an order of magnitude

[a]Permanent address: Laboratoire de Spectrometrie Ionique et Moleculaire (UMR No. 5579), CNRS et Universite Lyon I, 69622 Villeurbanne Cedex, France.
[b]Present address: Department of Chemistry, University of Indiana, Bloomington, IN 47405.

better than has been obtained using conventional injected-ion drift tube techniques.

Mobilities are measured by injecting a short pulse of ions into the drift tube and recording the arrival time distribution at the detector. Assuming that the pulse of ions is sufficiently short, the resolution in ion mobility measurements is limited by diffusion of the ion packet as it travels across the drift tube. The resolving power is given by[21]

$$\frac{t_{\mathrm{DT}}}{t_{1/2}} = \frac{1}{4}\left(\frac{ze}{k_B \ln 2}\right)^{1/2}\left(\frac{V}{T}\right)^{1/2}, \tag{1}$$

where t_{DT} is the drift time, $t_{1/2}$ is the width of the peak at half-height, ze is the charge on the ion, V is the voltage drop across the drift tube, and T is the temperature. It is apparent from Eq. (1) that in order to increase the resolving power it is necessary to increase the voltage across the drift tube. However, the buffer gas number density, N, is also an important parameter because it is desirable to keep the drifting ions in the low field limit, low E/N, where the mobility is independent of the drift field, E.[8] At high fields the mobility depends on the drift voltage and alignment of the drifting ions may occur. It is then considerably more difficult to relate the mobility to the geometry. So to substantially increase the voltage across the drift tube it is necessary to increase the buffer gas pressure. As the ions are injected into the drift tube, they undergo collisions with the buffer gas flowing out of the drift tube. If the buffer gas pressure is increased, then the injection energy must be increased to get the ions into the drift tube. A fraction of the ion's injection energy is converted into internal energy as they undergo collisions with the buffer gas at the drift tube entrance, and at high injection energies the ions fragment.[22] Thus, if the buffer gas pressure is raised substantially, it will not be possible to inject intact polyatomic ions into the drift tube. Our solution to this problem is to attach the source onto the beginning of the drift tube and to transfer ions directly from the source to the drift tube. A concern with this configuration is that neutral species should not be allowed to diffuse from the source into the drift tube because charge transfer may then occur in the drift tube and this could distort the measured drift time distributions. Our solution to this problem is to transfer the ions through an ion gate with a counterflowing buffer gas that prevents neutral species from entering the drift tube.

The design and construction of the apparatus are described in detail in Sec. II, and then several examples that illustrate the value of the increased resolving power are presented in Sec. III.

II. EXPERIMENTAL APPARATUS

Figure 1 shows a schematic diagram of the apparatus. It consists of four main regions: (1) the source, where the clusters are produced; (2) the ion gate, which connects the source to the drift tube and prevents neutral species from entering the drift tube; (3) the drift tube; and (4) the mass spectrometer and the ion detector. The apparatus is built around a $80\times60\times45$ cm 304 stainless steel vacuum chamber pumped by two 2000 $\ell\,\mathrm{s}^{-1}$ diffusion pumps (Edwards High Vacuum, Diffstak 250/2000M). The source and drift tube are mounted

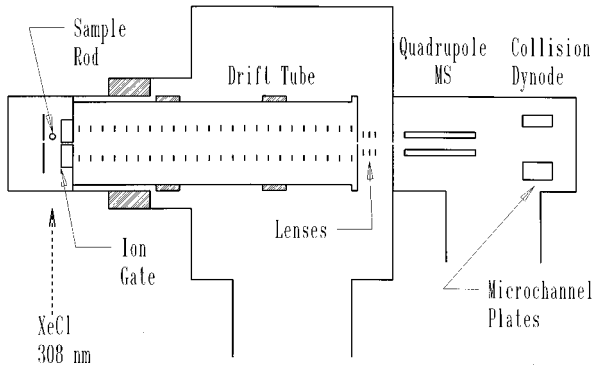

FIG. 1. Schematic diagram of the high-resolution ion mobility apparatus.

on one of the walls of the vacuum chamber and electrically isolated by a 7.5-cm-long G10 Garolite cylindrical spacer. During operation there is a potential difference of up to 14 000 V across the drift tube. The exit of the drift tube is at ground, and the source, the ion gate, and the entrance to the drift tube are at high voltage. The source and drift tube are operated with helium buffer gas (99.9999%) at around 500 Torr. Ions that exit the drift tube are focused through a 0.5-cm-diam aperture into a differentially pumped chamber housing a quadrupole mass spectrometer and an ion detector. This chamber is an 8-in.-diam. 304 stainless steel tee. It is pumped by a 700 $\ell\,\mathrm{s}^{-1}$ diffusion pump (Edwards High Vacuum, Diffstak 160/700M). The pressure during operation, as indicated by an uncalibrated ion gauge, is $\sim4\times10^{-5}$ Torr in the main chamber, and $\sim1\times10^{-6}$ Torr in the differentially pumped mass spectrometer region. The individual components of the apparatus are discussed in more detail below.

A. The source

The source is a novel laser vaporization/desorption source with a near static buffer gas. The buffer gas pressure in the source is around 500 Torr. An excimer laser (Lambda Physik 103 MSC) operating at 308 nm and focused with a 50 cm focal length lens was employed. Clusters are produced by laser vaporization of a 1/2-in.-diam target of the material to be studied. Silicon, NaCl, and a variety of metal clusters have been generated. Fullerenes and metallofullerenes were laser desorbed from a thin film deposited on a copper rod. To avoid boring a hole into it, the target is rotated and translated in a screw motion by a stepping motor located outside the vacuum chamber. The motor is connected to the target by an insulating fiberglass rod that enters the vacuum chamber via a differentially pumped feedthrough. Photomicrosensors are used to sense the position of the rod, and a microprocessor reverses its direction of travel when predetermined limits are reached. In a conventional laser-vaporization cluster source, the vaporized material is entrained by a flowing buffer gas that ultimately ejects the clusters from the source. With this new source, there is no buffer gas flow to entrain the clusters and guide them out of the source. Instead, cluster ions are guided from the target rod toward the entrance of the ion gate by a shaped electric field. Figure 2 shows the equipotential lines in the source as determined using SIMION.[23] In

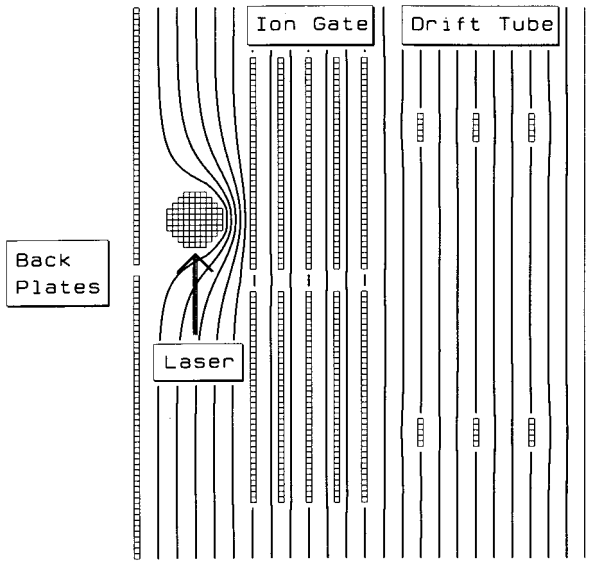

FIG. 2. Equipotential lines in the source, the ion gate, and the beginning of the drift tube as determined using SIMION. The equipotential lines are separated by 75 V. Only four out of the ten ion gate plates are shown. The arrow shows where the laser beam strikes the target rod.

the simulation, the potentials of the rod and the two back plates are equal. The potential of the rod is defined by two contacts with the plate immediately behind it. The potential difference between the rod and the entrance of the ion gate is typically around 600 V. The arrow shows the point where the laser strikes the target rod. Because of the high buffer gas pressure, the ions follow trajectories that are perpendicular to the equipotential lines. The rod was positioned so that the trajectories from the point where the laser strikes the target enter the ion gate. The signal can be optimized by adjusting the potential between the two back plates. By adjusting the voltage on the rod, one can adjust the residence time of the clusters in the source and vary the cluster size distribution. Only ionic species are extracted from the source. By reversing the voltages it is possible to extract either anions or cations.

B. The ion gate

The function of the ion gate is to allow ions to pass from the source into the drift tube while preventing neutral species from entering the drift tube. This is accomplished by a uniform electric field to carry the ions through the ion gate and a counterflow of buffer gas to prevent neutral species from passing through. The ion gate is a 2.4-cm-long cylindrical channel with an inside diameter of 0.5 cm. It consists of ten 304 stainless steel disks separated by Teflon sheets. The voltage difference between the entrance and the exit of the ion gate is typically 450 V. The metal disks are connected by 5 MΩ resistors (KDI Electronics, PVV60) in order to generate a uniform electric field along the length of the ion gate (see Fig. 2). The power supplies for the ion gate and the source float at the potential at the entrance of the drift tube so that the electric field in the drift tube can be easily changed without changing the voltages across the source or the ion gate.

Helium enters the drift tube through the grounded end plate, and the source is pumped by a liquid-nitrogen-trapped mechanical pump so that there is a small gas flow along the drift tube axis and a larger gas flow along the axis of the ion gate. The buffer gas flow into the drift tube and out of the source is regulated by two leak valves. The small pressure difference between the drift tube and the source, a fraction of a mTorr, is monitored by a differential capacitance manometer (MKS, baratron 223B). A series of simulations were performed to determine the dimensions of the ion gate and to establish the buffer gas flow and electric field required to allow ions to pass through the ion gate while preventing neutral species from entering the drift tube. The total buffer gas flow, around 1300 sccm, is monitored by a flow meter (MKS, 258C). Approximately 90% of the buffer gas flow passes through the ion gate while the balance leaves through the aperture in the drift tube exit plate. Under these conditions we see no evidence for neutral species entering the drift tube.

C. The drift tube

The drift tube is housed in a 6-in.-diam 304 stainless steel tube with two ceramic breaks (Ceramaseal) along the length. The total length of the drift tube is 63 cm. A uniform electric field is generated along the axis of the drift tube by 43 0.010-in.-thick copper beryllium drift guard rings separated by ceramic spacers. A voltage divider consisting of a chain of 5 MΩ resistors (KDI Electronics, PVV60) provides the potentials to the drift guard rings. At the end of the drift tube the ions are carried by the buffer gas through a 0.005-in.-diam hole into the vacuum chamber. The first section of the outer wall of the drift tube is connected to the high voltage at the drift tube entrance, the middle section to the middle drift guard ring, and the last section to the exit plate. This design minimizes the potential difference between any drift guard ring and the walls of the tube, and reduces the possibility of a discharge inside the drift tube. The maximum voltage that can be used across the drift tube depends on the pressure. The breakdown voltage decreases as the helium pressure increases; it has a minimum at around 4 cm Torr, and then increases.[24] With 500 Torr in the drift tube, a drift voltage of up to 14 000 V can be used. Each stainless steel section of the drift tube is surrounded by a jacket for heating or cooling. The drift tube guard rings were designed to have a small heat capacity to minimize the time required to bring the system to thermal equilibrium. We have employed a temperature-regulated recirculator (Neslab, RT-40) with a nonconducting fluorocarbon fluid (3M, FC40) to control the temperature. Using this arrangement we have performed measurements in the temperature range from −25 to +100 °C. A temperature range from −40 to +400 °C should be accessible with suitable heat-transfer fluids.

D. Mass analysis and detection

After exiting the drift tube, the ions are accelerated and focused by a set of electrostatic lenses. The ions are directed through a 0.5-cm-diam aperture into a differentially pumped chamber that houses a quadrupole mass spectrometer and an

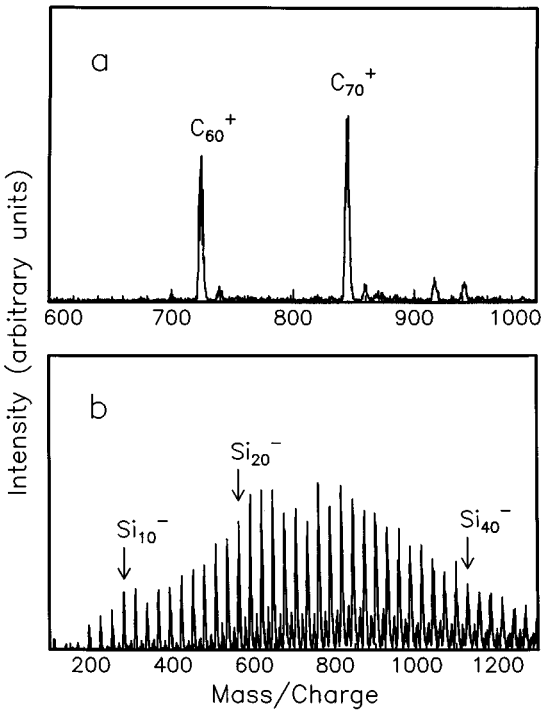

FIG. 3. Mass spectra measured for (a) laser desorbed fullerene film and (b) silicon cluster anions generated by laser vaporization. The small peaks between the silicon peaks correspond to Si_nO^- clusters.

ion detector. The quadrupole mass spectrometer (Extrel) has 3/8-in.-diam rods and is operated at 880 kHz to provide a upper mass limit of 4000 amu. At the end of the quadrupole, ions are detected by an off-axis collision dynode and dual microchannel plates. The collision dynode is biased at +10 000 V for anions and −10 000 V for cations. Signals from the microchannel plates are processed with a fast preamplifier (EG&G Ortec, VT120A) and a fast amplifier/discriminator (EG&G Ortec, 9307). The signals are then recorded with a 66 MHz 486 computer (Gateway). To record mass spectra, a 16 bit digital/analog (D/A) converter (Analog Devices, DAC1136) is used to drive the quadrupole mass spectrometer and a counter board (Computer Boards, CIO-CTR05) is used to record the signal at a particular mass. Drift time distributions are recorded by measuring the arrival time distribution at the detector using a multichannel scaler board (Tennelec/Nucleus, MCS II), with a start pulse provided by the vaporization laser.

III. RESULTS

A. Mass spectra

Figure 3(a) shows a mass spectrum obtained by laser desorption (~200 μJ/pulse) of a fullerene film containing a mixture of fullerenes. The two main peaks correspond to C_{60}^+ and C_{70}^+. The mass resolved signals were around 1000 counts/s at a laser pulse frequency of 100 Hz. Figure 3(b) shows the mass spectrum recorded for silicon cluster anions generated by pulsed laser vaporization (~10 mJ/pulse) of a silicon rod. Si_n^- clusters in the size range $n=4$–45 are present in Fig. 3(b). The high mass peaks are broadened by the presence of the silicon's three isotopes (28 amu, 92.2%; 29 amu, 4.7%; and 30 amu, 3.1%). A mass resolved signal of several hundred counts/s is observed with a laser pulse frequency of 100 Hz. The cluster size distribution is sensitive to the laser power, the focusing of the laser, and the voltages on the source. These parameters can be adjusted to optimize the signal for small clusters or to produce clusters with more than 100 silicon atoms.

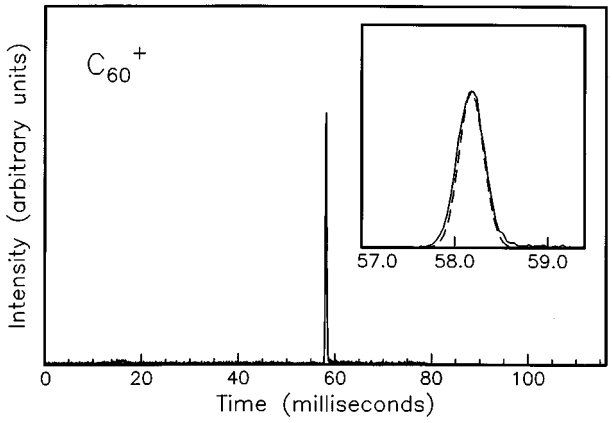

FIG. 4. Arrival time distribution measured for C_{60}^+ with a drift voltage of 10 000 V. The inset shows a comparison of the measured peak (solid line) and the peak shape calculated for the diffusion of an ion packet as it travels through the drift tube (dashed line; see the text, Sec. III C).

B. Drift time distributions

Figure 4 shows an arrival time distribution recorded for C_{60}^+. This distribution was measured at room temperature, with a pressure of 506 Torr in the drift tube, and a drift voltage of 10 000 V. A single sharp peak is observed. The arrival time, t, of the fullerene is 58.16 ms. The zero time is determined by the laser pulse. The arrival time corresponds to the total time from the desorption of the fullerenes by the laser to their detection; it can be resolved into four components:

$$t=t_S+t_{\mathrm{IG}}+t_{\mathrm{DT}}+t_V, \tag{2}$$

where t_S is the time spent in the source, t_{IG} is the time spent in the ion gate, t_{DT} is the time spent in the drift tube, and t_v is the time spent from the exit of the drift tube to the detector. The time spent in the drift tube is inversely proportional to the electric field in this region, E_{DT}:

$$t_{\mathrm{DT}}=\frac{l_{\mathrm{DT}}}{KE_{\mathrm{DT}}}, \tag{3}$$

where l_{DT} is the length of the drift tube and K is the mobility of the ion. Figure 5 shows a plot of the arrival times measured for C_{60}^+ as a function of the inverse of the drift voltage. A straight line is observed. This shows that the mobility is independent of the drift field, and indicates that the conditions employed are in the low field limit. The slope of the line is proportional to the inverse mobility of the cluster. Mobilities are usually reported as a reduced mobility given by[8]

$$K_0=K\,\frac{p}{760}\,\frac{273.16}{T}, \tag{4}$$

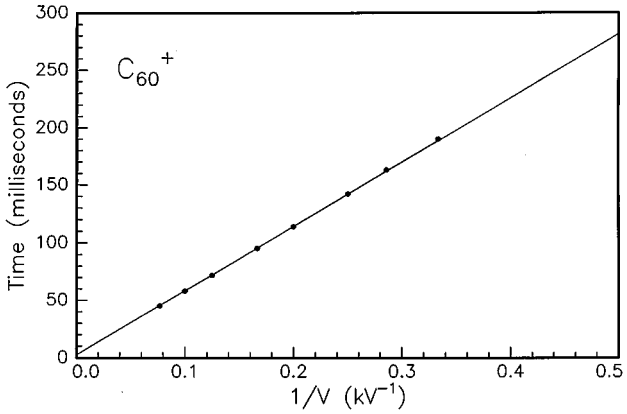

FIG. 5. Arrival time of C_{60}^+ plotted as a function of the inverse of the drift voltage for drift voltages in the range of 3000–13 000 V. The line is a linear least-squares fit to the data. The slope of the line is 558 ms kV and the intercept is 2.6 ms.

where T and p are, respectively, the temperature and the pressure in the drift tube. The reduced mobility determined from the data in Fig. 5 is $K_0=4.321\pm0.040$ cm^2 V^{-1} s^{-1}. This can be compared with the value obtained for the mobility of C_{60}^+ using the injected-ion drift tube apparatus in our laboratory, 4.31 cm^2 V^{-1} s^{-1}. We estimate that the absolute uncertainty of reduced mobilities determined with this new apparatus is $\pm1\%$. Independent measurements are reproducible within less than 0.2%.

The intercept in Fig. 5 corresponds to the time that the ions do not spend in the drift tube. This time is 2.6 ms. It consists of the time spent in the source, the ion gate, and the time spent traveling to the detector after exiting the drift tube. These three times can be calculated. The times spent in the source and in the ion gate depend on the mobility of the ion, and they can be calculated with expressions similar to Eq. (3). The time spent traveling from the drift tube exit plate to the detector, t_v, can be calculated from the mass of the ion, the charge of the ion, and the voltages applied to the quadrupole and the lenses. Thus the total time can be written as

$$t=\frac{1}{K}\left(\frac{l_S}{E_S}+\frac{l_{\mathrm{IG}}}{E_{\mathrm{IG}}}+\frac{l_{\mathrm{DT}}}{E_{\mathrm{DT}}}\right)+t_V, \tag{5}$$

where l_S and l_{IG} are the distances traveled in the source and in the ion gate, respectively, and E_S and E_{IG} correspond to the electric fields in these regions. l_S and E_S were estimated using the equipotentials plotted in Fig. 2. The times spent in the source, ion gate, drift tube, and traveling to the detector, with the conditions used to record the drift time distribution that is shown in Fig. 4, are given in Table I. Note that, by using Eq. (5), the mobility can be obtained directly from a single drift time distribution.

TABLE I. Times spent by the C_{60}^+ fullerene in the different parts of the apparatus. These times correspond to the conditions used to record the distribution shown in Fig. 4.

	Source	Ion gate	Drift tube	Vacuum	Total
Time (ms)	0.52	1.80	55.50	0.34	58.16

C. Resolution

The time distribution of the packet of ions at the exit of the drift tube depends on the spatial and temporal distribution of ions generated in the source and the spatial dispersion that occurs as the ions travel through the drift tube. The ion packet spreads out as the ions travel through the drift tube because of diffusion. If one assumes that all the ions are produced in the source at the same time, the shape of the drift time distribution can be calculated using the following relation:[8]

$$\Phi(t)=\frac{\Phi_0}{\sqrt{4\pi Dt}}\,(1-e^{-r_0^2/4\mathrm{Dt}})e^{-(l_{\mathrm{DT}}-\nu_{\mathrm{DT}}t)^2/4\mathrm{Dt}}, \tag{6}$$

where D is the diffusion constant which under low field conditions is given by eK/k_BT, v_{DT} is the drift velocity in the drift tube, and r_0 is the radius of the source of ions. We have used the radius of the ion gate and the radius of the laser spot for r_0. Both radii give essentially the same result. The calculated distribution for C_{60}^+ is plotted as the dashed line in the inset of Fig. 4. The measured peak is slightly broader than the calculated one. This is probably due to the initial spatial distribution of the ions. While the ions are generated by the laser pulse at the same time, they are not produced at exactly the same position. Ions generated at slightly different positions are subjected to slightly different electric fields in the source, and so they enter the drift tube at slightly different times. When a small laser spot is employed, as in Fig. 4, this effect is negligible. However, a significant broadening of the peak is observed if a large laser spot is used and if the difference in voltage between the rod and the ion gate is small ($\sim$100 V instead of $\sim$600 V). The width at half-height of the peak shown in Fig. 4 is $t_{1/2}=0.34$ ms. The resolving power, $t_{\mathrm{DT}}/t_{1/2}$, is 172. Isomers with mobilities that differ by more than 0.5% are easily separated in this apparatus.

Figure 6 shows drift time distributions recorded for laser desorbed $Sc_2C_{82}^+$ on a conventional injected-ion drift tube apparatus and on the new high-resolution drift tube apparatus. The dashed line corresponds to the distribution measured with the conventional apparatus whereas the solid line shows that recorded with the high-resolution apparatus. The results of ion mobility measurements for Sc at C_n^+, Sc_2 at C_n^+, and Sc_3 at C_n^+ metallofullerenes will be reported elsewhere. The drift tube in the injected-ion drift tube apparatus is 7.6 cm long, the drift voltage is 100 V, and the helium buffer gas pressure is 5 Torr. The resolving power of this drift tube is 17. The resolving power with the high-resolution apparatus, with a drift voltage of 10 000 V, is an order of magnitude higher. While only one broad peak is observed with the conventional apparatus, the inset shows that two peaks are resolved with the new apparatus. The difference in the drift times of these two peaks is 1.3%. The two peaks correspond to two different isomers with very similar shapes. The reduced mobilities of these isomers are 3.571 and 3.524 cm^2 V^{-1} s^{-1}. For comparison the reduced mobility of C_{82}^+ is 3.530 cm^2 V^{-1} s^{-1}.

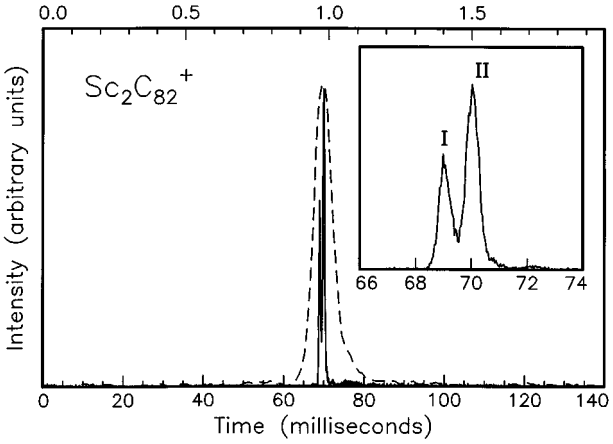

FIG. 6. Drift time distribution measured for laser desorbed $Sc_2C_{82}^+$ using the high-resolution ion mobility apparatus with a drift voltage of 10 000 V (solid line). The distribution recorded with a conventional injected-ion drift tube apparatus with a drift voltage of 100 V is shown for comparison (dashed line). The time scale for the distribution measured with the high-resolution apparatus is at the bottom, and the time scale for the distribution recorded with the injected-ion-drift tube apparatus is shown at the top of the plot. The distribution measured with the high-resolution apparatus is enlarged in the inset and shows two clearly resolved peaks.

Figure 7 shows a drift time distribution measured for Si_{30}^-. For this cluster five different isomers are resolved, and some of the peaks appear to consist of more than one component. In previous experiments with the injected-ion drift tube apparatus only two isomers were resolved.[14] Combined reactivity/ion mobility measurements suggested that more than two isomers exist for certain cluster sizes.[11] With the high-resolution apparatus new isomers were observed for all silicon clusters with 20–70 atoms; up to seven isomers are resolved for some cluster sizes.[25] This is the first evidence to indicate that such a large number of isomers can exist for these clusters, and demonstrates the need for high-resolution ion mobility measurements.

D. Study of structural interconversion in the drift tube

Multiple isomers were observed for many of the clusters that we have studied. Metastable geometries can be formed

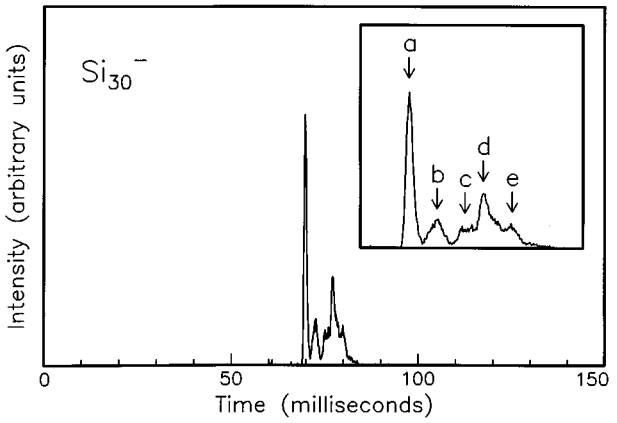

FIG. 7. Drift time distribution measured for Si_{30}^- with a drift voltage of 10 000 V. Five isomers are resolved.

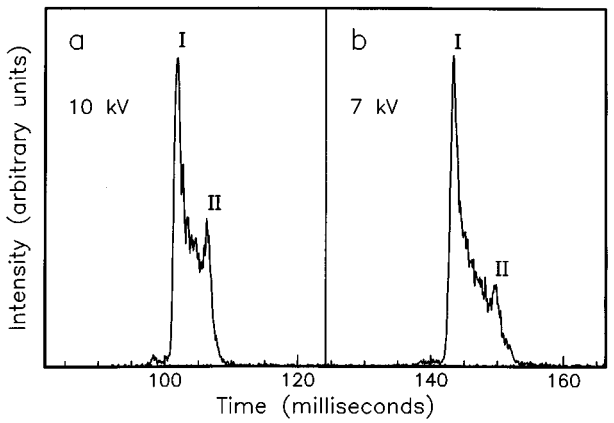

FIG. 8. Drift time distributions measured for $(NaCl)_{23}Na^+$ clusters with drift voltages of (a) 10 000 and (b) 7000 V. The drift tube temperature was −14 °C.

during cluster growth and they may not relax to the most stable structure. While the identification of the different isomers is important, it is perhaps more important to determine the most stable structure. In an injected-ion drift tube apparatus the clusters may be annealed by raising the injection energy so that the ions become collisionally heated as they enter the drift tube.[17] This approach has been used to examine the isomerization processes of silicon clusters[14] and carbon clusters.[18] For carbon, important information about the mechanism of fullerene formation was deduced from these annealing studies. In the high-resolution ion mobility apparatus, the ions are not injected into the drift tube, and so it is not possible to raise the injection energy. However, the clusters can be annealed using a laser[26] or annealed by raising the temperature of the drift tube.[27] We have previously employed these methods with the injected-ion drift tube apparatus, and both of them can be implemented with the high-resolution ion mobility apparatus. Laser annealing experiments can be performed with the laser beam perpendicular to the axis of the drift tube, to irradiate a particular isomer, or with the laser beam along the axis of the drift tube. Below we briefly describe some annealing experiments performed by changing the temperature of the drift tube.

With the high buffer gas pressure employed in the high-resolution drift tube apparatus, ions undergo 10^8–10^{10} collisions/s, and they spend around 10^{-1} s in the drift tube with a drift voltage of 10 000 V. If the temperature of the drift tube is raised, then isomerization can occur by a thermally activated unimolecular reaction. By monitoring the isomerization processes as a function of the drift voltage, at a fixed drift tube temperature, it is possible to determine rate constants for the isomerization processes. If the rate constants are measured as a function of the temperature, then the activation energy can be deduced from an Arrhenius plot. By lowering the drift voltage, isomerization processes can be studied over a time period as long as 1 s. Figure 8 shows drift time distributions recorded for $(NaCl)_{23}Na^+$ with drift voltages of 7000 and 10 000 V. Both distributions were recorded with a drift tube temperature of −14 °C. Two poorly resolved peaks, corresponding to two different isomers, are observed in each distribution. The peaks are poorly resolved

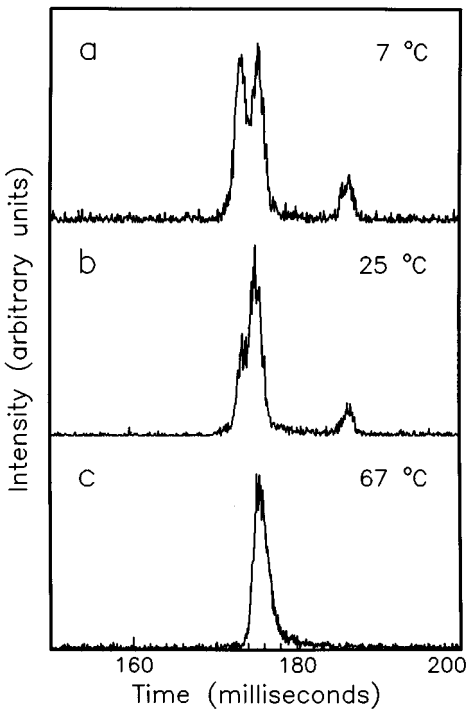

FIG. 9. Drift time distributions measured for $(NaCl)_{35}Cl^-$ clusters with drift tube temperatures of 7, 25, and 67 °C and a drift voltage of 7000 V. The time scale corresponds to that for the distribution measured at 25 °C. The drift times depend on the temperature, and the time scales for the other two distributions were scaled so that the peaks are aligned. Three isomers are observed at 7 °C, while only one isomer is observed at 67 °C.

because the isomers are interconverting as they travel through the drift tube. At room temperature, where the rate of isomerization is higher, only one peak is observed. It is obvious from Fig. 8 that the ratio of the two peaks changes as the drift voltage is changed. The relative abundance of isomer II is lower in the distribution recorded with a drift voltage of 7000 V because with this lower drift voltage more time is available for conversion of isomer II into isomer I. With an even lower drift voltage, most of isomer II isomerizes before the exit of the drift tube. These results indicate that isomer I is the more stable isomer.

Figure 9 shows drift time distributions of $(NaCl)_{35}Cl^-$ measured for three different drift tube temperatures. While at 7 °C three different isomers are observed; only one isomer is observed at 67 °C. At 7 °C, activation barriers prevent isomerization. As the temperature increases, the isomerization rate increases. At 67 °C, only the most stable isomer remains. The isomerization rate constants can be determined, as a function of temperature, by simulating the drift time distributions.[28] The observed $(NaCl)_nCl^-$ clusters have cuboid geometries, and the isomers observed correspond to cuboids with different $jxkxl$ dimensions. The isomerization processes thus correspond to interconversion between cuboid geometries with different $jxkxl$ dimensions. It is remarkable that these structural transformations occur at such low temperatures.

IV. DISCUSSION

We have described a new apparatus for performing high-resolution ion mobility measurements for gas phase ions. The apparatus operates with a drift voltage of up to 14 000 V at a buffer gas pressure of 500 Torr. Since it is not possible to inject intact ions into such a high buffer gas pressure, a novel laser desorption/vaporization source is coupled directly to the drift tube through an ion gate. The ion gate prevents neutral species from entering the drift tube from the source region. A resolving power of 172 is obtained with a drift voltage of 10 000 V. This is very close to the diffusion limit. Mobilities can be measured with an absolute accuracy of $\pm 1\%$ and values are reproducible within 0.2%. The drift tube temperature can be changed to study thermally activated isomerization processes as a function of temperature. Rate constants for the isomerization processes can be obtained from the drift time distributions, and activation energies can be determined from an Arrhenius plot. At low drift fields, isomerization processes can be monitored over a 1 s time scale. Results obtained for metallofullerenes, silicon clusters, and $(NaCl)_nCl^-$ and $(NaCl)_nNa^+$ clusters illustrate the value of high-resolution ion mobility measurements in resolving structural isomers. In the future we intend to attach an electrospray ion source to the apparatus so that high-resolution ion mobility measurements can be used to examine the structure and folding of gas phase proteins. In addition, with the cluster signals available from this apparatus it will be possible to attach a magnetic-bottle photoelectron spectrometer in back of the mass spectrometer, so that anion photoelectron spectra can be recorded for the isomers resolved in the ion mobility measurements.

ACKNOWLEDGMENTS

The metallofullerene samples used in these studies were graciously provided by Dr. T. Sugai and Professor H. Shinohara. The authors gratefully acknowledge the National Science Foundation (CHE-9306900) and the Petroleum Research Fund (administered by the American Chemical Society) for support of this work. One author (Ph.D.) also acknowledges the support of the Centre National de la Recherche Scientifique (CNRS).

[1] D. F. Hagen, Anal. Chem. **51**, 870 (1979).
[2] B. R. Rowe, D. W. Fahey, F. C. Fehsenfeld, and D. L. Albritton, J. Chem. Phys. **73**, 194 (1980).
[3] M. J. Cohen and F. W. Karasek, J. Chromatogr. Sci. **8**, 330 (1970).
[4] R. H. St. Louis and H. H. Hill, Crit. Rev. Anal. Chem. **21**, 321 (1990).
[5] H. H. Hill, W. F. Siems, R. H. St. Louis, and D. G. McMinn, Anal. Chem. **62**, 1201A (1990).
[6] M. D. Wessel and P. C. Jurs, Anal. Chem. **66**, 2480 (1994).
[7] K. T. Whitby and W. E. Clark, Tellus **18**, 573 (1966); T. M. Sanders and S. R. Forest, J. Appl. Phys. **66**, 3317 (1989).
[8] E. A. Mason and E. W. McDaniel, *Transport Properties of Ions in Gases* (Wiley, New York, 1988).
[9] V. Nestler, B. Betz, and P. Warneck, Ber. Bunsenges. Phys. Chem. **81**, 13 (1977); R. Thomas, A. Barassin, and R. R. Burke, Int. J. Mass Spectrom. Ion Phys. **28**, 275 (1978); W. Lindinger, E. Alge, H. Stori, R. N. Varney, H. Helm, P. Holzmann, and M. Pahl, Int. J. Mass Spectrom. Ion Phys. **30**, 251 (1979); R. Johnson, M. A. Biondi, and M. J. Hatashi, J. Chem. Phys. **77**, 2545 (1982); F. Bohringer and F. Arnold, J. Chem. Phys. **77**, 5534 (1982).
[10] Y. Kaneko, M. R. Megill, and J. B. Hasted, J. Chem. Phys. **45**, 3741 (1966).
[11] M. F. Jarrold, J. Phys. Chem. **99**, 11 (1995).
[12] G. von Helden, M.-T. Hsu, P. R. Kemper, and M. T. Bowers, J. Chem.

Phys. **93**, 3835 (1991); G. von Helden, M.-T. Hsu, N. Gotts, and M. T. Bowers, J. Chem. Phys. **97**, 8182 (1993).
[13] K. B. Shelimov, J. M. Hunter, and M. F. Jarrold, Int. J. Mass Spectrom. Ion Phys. **138**, 17 (1994); J. M. Hunter and M. F. Jarrold, J. Am. Chem. Soc. **117**, 103 (1995).
[14] M. F. Jarrold and V. A. Constant, Phys. Rev. Lett. **67**, 2994 (1991).
[15] J. M. Hunter, J. L. Fye, M. F. Jarrold, and J. E. Bower, Phys. Rev. Lett. **73**, 2063 (1994).
[16] D. E. Clemmer, J. M. Hunter, K. B. Shelimov, and M. F. Jarrold, Nature (London) **372**, 248 (1994); G. von Helden, N. G. Gotts, P. Maitre, and M. T. Bowers, Chem. Phys. Lett. **227**, 601 (1994).
[17] M. F. Jarrold and E. C. Honea, J. Am. Chem. Soc. **114**, 459 (1992).
[18] J. M. Hunter, J. L. Fye, and M. F. Jarrold, Science **260**, 784 (1993); G. von Helden, N. G. Gotts, and M. T. Bowers, Nature (London) **363**, 60 (1993).
[19] G. von Helden, T. Wyttenbach, and M. T. Bowers, Science **267**, 1483 (1995).
[20] D. E. Clemmer, R. R. Hudgins, and M. F. Jarrold, J. Am. Chem. Soc. **117**, 10141 (1995); K. B. Shelimov, D. E. Clemmer, R. R. Hudgins, and M. F. Jarrold, *ibid.* (in press).
[21] H. E. Rivercomb and E. A. Mason, Anal. Chem. **47**, 970 (1975).
[22] M. F. Jarrold and E. C. Honea, J. Phys. Chem. **95**, 9181 (1991).
[23] Simion Ver. 6.0s, Idaho National Engineering Laboratory.
[24] J. M. Meek and J. D. Craggs, *Electrical Breakdown of Gases* (Oxford University Press, London, 1953).
[25] Ph. Dugourd, R. R. Hudgins, and M. F. Jarrold (to be published).
[26] J. M. Hunter, K. B. Shelimov, and M. F. Jarrold (unpublished).
[27] M. F. Jarrold and J. E. Bower, J. Phys. Chem. **98**, 2399 (1993).
[28] R. R. Hudgins, Ph. Dugourd, J. M. Tenebaum, and M. F. Jarrold (to be published).